10^{th} South African Conference on Computational and Applied Mechanics
Potchefstroom
3-5 October 2016

Cyclic effects and recrystallisation in temperature and rate dependent state variable based plasticity

G.J. Jansen van Rensburg[1,2,*], S. Kok[2], D.N. Wilke[2]

[1]Advanced Mathematical Modelling, Modelling and Digital Sciences, CSIR, South Africa
[2]Department of Mechanical and Aeronautical Engineering, University of Pretoria, South Africa

[*]jjvrensburg@csir.co.za

ABSTRACT

A constitutive model that captures the dominant strengthening and softening physics or microstructural changes of metallic materials is needed within a numerical environment for the effective prediction and simulation of plasticity during hot working processes. Dislocation density or related stress values play the primary role of internal state dependent variables in the development of many unified constitutive material models using the Kocks-Mecking work hardening theory as foundation. This theory is based on an approach to model the viscoplastic behaviour of crystalline materials as a result of interaction between mobile and forest dislocations in the material microstructure. Dislocation density based state dependent models have the ability to not only provide a good description of the mechanical response of metallic materials in uniform loading, but also have good predictive capability. One popular model is the Mechanical Threshold Stress model while other dislocation kinetics based models have also been proposed in literature to include various physical phenomena. In this conference contribution, the development and implementation of temperature and rate dependent state variable based plasticity is presented. The model foundation as well as extensions to include cyclic effects and recrystallisation are coded into a user material subroutine for use in finite element packages.

KEYWORDS

Mechanical Threshold Stress, dislocation density based material modelling, combined hardening, recrystallisation

INTRODUCTION

Most Finite Element Analysis (FEA) software packages have a comprehensive list of material models already implemented to choose from. If a different material model is required, a user implemented material subroutine can be linked to Abaqus, CalculiX and Code_Aster for example. All three of these packages can make use of the Abaqus user material format coded in Fortran. Sophisticated state variable based models such as the Mechanical Threshold Stress (MTS) model [1] as well as dislocation density based combined isotropic and kinematic hardening [2] or models for static and dynamic recrystallisation [3] are available in the research space. Many of these models can be seen as implementations and extensions using the Kocks-Mecking hardening theory [4, 5, 6, 7] as foundation.

The development and implementation of state dependent user materials in computational plasticity is discussed in the Ph.D. thesis by Jansen van Rensburg [8]. In the thesis, an incrementally objective user material framework for purely isotropic and kinematic hardening J_2 plasticity is developed, implemented and verified against the native implementation of Abaqus. These user material frameworks can be extended by altering either the purely isotropic or combined hardening subroutines as well as the support functions called by the framework, resulting in an array of more sophisticated models.

Within the implemented framework for user material subroutines, the MTS model as well as dislocation density based extensions are presented in this paper. Coding of these scalar equations into purely isotropic or combined hardening subroutines result in incrementally objective implementations of the models for use in FEA [8].

THE MECHANICAL THRESHOLD STRESS MODEL

The MTS model was developed by Follansbee and Kocks [1] to describe the post yielding behaviour of metals. In the MTS model, the mechanical threshold ($\hat{\sigma}$) is the internal state variable. This threshold value represents a theoretical maximum flow stress at 0K. From there the material flow stress, σ_{Y}, is obtained by scaling the mechanical threshold to accommodate rate and temperature dependence. Following Nabarro et al. [9], the threshold flow stress is separated into an athermal $\hat{\sigma}_a$ and k different thermal components $\hat{\sigma}_T^k$. At different absolute temperature values T and plastic strain rates $\dot{\varepsilon}_{\mathrm{p}}$, the contribution to the flow stress σ_T^k is related to the threshold counterpart $\hat{\sigma}_T^k$ through the scaling function $S_k(\dot{\varepsilon}_{\mathrm{p}}, T)$, so that

$$\sigma_T^k = \hat{\sigma}_T^k \frac{\mu\,(T)}{\mu_r} S_k(\dot{\varepsilon}_{\mathrm{p}}, T). \tag{1}$$

Here, $\mu\,(T)$ and μ_r indicate the current and reference shear modulus values. The temperature dependent shear modulus is expressed by Varshni [10] as

$$\mu(T) = \mu_r - \frac{D_r}{\exp\left(T_r/T\right) - 1}, \tag{2}$$

where μ_r, D_r and T_r are constants. The reference temperature T_r has to be well below the temperatures of interest. The scaling functions take the form [1]

$$S_k(\dot{\varepsilon}_{\mathrm{p}}, T) = \left[1 - \left(\frac{k_{\mathrm{B}} T}{g_{0k}\mu b^3} \ln \frac{\dot{\varepsilon}_{0k}}{\dot{\varepsilon}_{\mathrm{p}}}\right)^{1/q_k}\right]^{1/p_K}, \tag{3}$$

where g_{0k} is the normalised activation energy for dislocations to overcome the obstacles, b is the magnitude of the Burgers' vector length and $k_{\mathrm{B}} = 1.38064852{\times}10^{-23}\mathrm{m^2kgs^{-2}K^{-1}}$ is the Boltzmann constant. $\dot{\varepsilon}_{0k}$ is a constant proportional to the density of mobile dislocations while p_k and q_k are statistical constants that characterise the shape of the obstacle profile. In the original MTS model, two thermal stresses are used, i.e. $\hat{\sigma}_T^1$ and $\hat{\sigma}_T^2$. The first is a constant thermal stress $\hat{\sigma}_i = \hat{\sigma}_T^1$. The second is an evolving threshold stress internal state variable $\hat{\sigma}_\varepsilon = \hat{\sigma}_T^2 = \frac{1}{2} M\mu b\sqrt{\rho}$ with M the average Taylor factor that accounts for the polycrystallinity of the material [5]. The equivalent flow stress σ_{Y} is finally expressed as

$$\sigma_{\mathrm{Y}} = \hat{\sigma}_a + \hat{\sigma}_i \frac{\mu\,(T)}{\mu_r} S_i(\dot{\varepsilon}_{\mathrm{p}}, T) + \hat{\sigma}_\varepsilon \frac{\mu\,(T)}{\mu_r} S_\varepsilon(\dot{\varepsilon}_{\mathrm{p}}, T). \tag{4}$$

The temperature and rate dependent evolution of the internal stress value in the presence of additional equivalent plastic strain according to the Kocks-Mecking work hardening theory can take the form [5]

$$\frac{d\hat{\sigma}_\varepsilon}{d\varepsilon_{\mathrm{p}}} = \frac{M\mu b}{4\sqrt{\rho}} \frac{d\rho}{d\varepsilon_{\mathrm{p}}} \quad \text{where} \quad \frac{d\rho}{d\varepsilon_{\mathrm{p}}} = Mk_1\sqrt{\rho} - Mk_2(\dot{\varepsilon}_{\mathrm{p}}, T)\,\rho. \tag{5}$$

The initial work hardening θ_0 as well as the temperature and rate dependent saturation stress $\hat{\sigma}_s\,(\dot{\varepsilon}_{\mathrm{p}}, T)$ can be introduced with

$$\theta_0 = \frac{M^2\mu b k_1}{4} \qquad \text{and} \qquad \hat{\sigma}_s\,(\dot{\varepsilon}_{\mathrm{p}}, T) = \frac{2\theta_0}{Mk_2(\dot{\varepsilon}_{\mathrm{p}}, T)}. \tag{6}$$

This means that the evolution of the threshold stress value $\hat{\sigma}_T$ could be expressed as a function of itself. This substitution results in the Voce-law [11]. Adding an exponent α results in the modified form of the Voce-law [11].

$$\frac{d\hat{\sigma}_\varepsilon}{d\varepsilon_{\mathrm{p}}} = \theta_0 \left(1 - \frac{\hat{\sigma}_\varepsilon}{\hat{\sigma}_s}\right)^\alpha. \tag{7}$$

Following the work of Chen and Gray [12], the threshold saturation stress $\hat{\sigma}_s\left(\dot{\varepsilon}_{\mathrm{p}}, T\right)$ is a function of both strain rate and temperature, through

$$\ln \frac{\dot{\varepsilon}_{\mathrm{p}}}{\dot{\varepsilon}_{0s}} = \frac{g_{0s}\mu b^3}{k_{\mathrm{B}}T} \ln \frac{\hat{\sigma}_s}{\hat{\sigma}_{0s}}, \tag{8}$$

where $\dot{\varepsilon}_{0s}$, g_{0s} and $\hat{\sigma}_{0s}$ are constants. The version of the MTS model contained in this section is implemented to work within the purely isotropic user material subroutine in [8]. The model is calibrated to hardening data at different strain rates and temperatures digitised from the work done by Tanner and McDowell [13] using a material point simulation. To compare the model response using a detailed Abaqus simulation to the data, compression of an axi-symmetric billet is modelled with material response provided by the user material. An axi-symmetric quarter of a billet is modelled using a 20×20 grid of quadratic axi-symmetric elements. The billet is compressed using a rigid analytical plane for the die contact surface. Hard normal contact between the billet and die is modelled with a Coulomb friction coefficient $\mu_{\mathrm{frict}} = 0.2$.

Four different problems are simulated that correspond to the experimental test data for $1\mathrm{s}^{-1}$ and $0.0004\mathrm{s}^{-1}$ at 298K, $0.0004\mathrm{s}^{-1}$ at 407K and $0.01\mathrm{s}^{-1}$ at 542K. The billet section modelled has a radius of 2.5mm and a half length of 5mm, meaning a 100% reduction in length corresponds to a die displacement of 5mm $\times$ $(\exp(-1) - 1) = -3.1606$mm. This displacement is applied over 1s in the $1\mathrm{s}^{-1}$ case, 100s in the $0.01\mathrm{s}^{-1}$ case and 2500s in the $0.0004\mathrm{s}^{-1}$. The simulations are solved over 100 time increments.

The material property values used in the simulation are itemised below.

- The elastic property values of $\mu_r = 49.91$GPa, $D_r = 3.29$GPa and $T_r = 200$K in Equation (2) are used with a Poisson's ratio of $\nu = 1/3$.
- The stress values in Equation (4) are $\hat{\sigma}_a = 0$MPa, $\hat{\sigma}_i = 20.67$MPa and $\hat{\sigma}_\varepsilon|_{\varepsilon_{\mathrm{p}}=0} = 0$MPa.
- The scaling function values in Equation (3) are $k_{\mathrm{B}}/g_{0i}b^3 = 1.402$MPa/K, $k_{\mathrm{B}}/g_{0\varepsilon}b^3 = 1.632$MPa/K, $p_\varepsilon = p_i = q_\varepsilon = q_i = 1$ and $\dot{\varepsilon}_{0\varepsilon} = \dot{\varepsilon}_{0i} = 10^7\mathrm{s}^{-1}$.
- The power law hardening according to Equation (7) is used with $\theta_0 = 2611.94$MPa and $\alpha = 2$.
- The saturation stress in Equation (8) have property values $\hat{\sigma}_{0s} = 689.12$MPa, $k_{\mathrm{B}}/g_{0s}b^3 = 0.5011$MPa/K and $\dot{\varepsilon}_{0s} = 10^{10}$.

In Figure 1, the von Mises stress distributions after 100% reduction in length is displayed for the hardest and softest of the material responses modelled. In Figure 1(a) the $1\mathrm{s}^{-1}$ at 298K results are given while (b) is the stress distribution in the $0.01\mathrm{s}^{-1}$ at 542K case. From the Abaqus results, the true strain values at each increment is determined from the prescribed die displacement. The volume preserving area assumption is further used to calculate the true stress using the reaction force extracted at the mid plane nodes. In Figure 1(c) the effective stress versus strain curves for the four cases simulated are presented compared to the experimental data of Tanner and McDowell [13].

The Abaqus simulation data with simple post processing to estimate the true stress - true strain data compares well to the experimental test data. The non-smooth response starting at about $\varepsilon \approx 0.5$ is due to the contact between the die surface and rollover of elements at the corner. If greater accuracy between the finite element result and experimental test data is required however, further characterisation using numerical optimisation can be performed using finite element evaluations within the objective function evaluation.

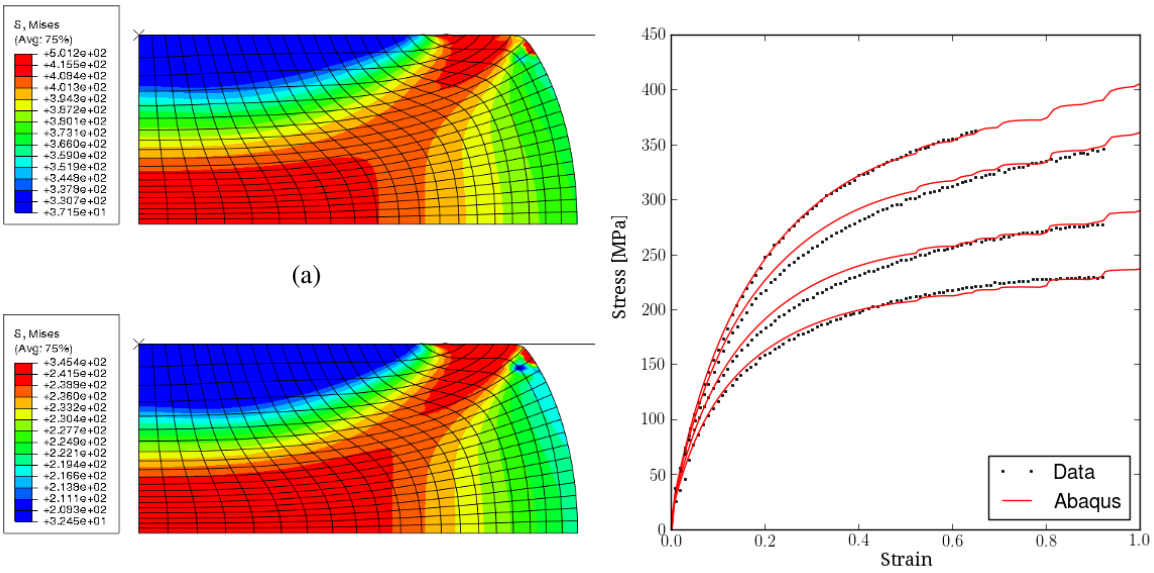

Figure 1: Von Mises stress distributions after 100% reduction in length for (a) 1s^{-1} at 298K and (b) 0.01s^{-1} at 542K. (c) Abaqus axi-symmetric simulation response using the material parameters estimated for OFHC Cu compared to the experimental test data in descending order for 1s^{-1} and 0.0004s^{-1} at 298K, 0.0004s^{-1} at 407K and 0.01s^{-1} at 542K.

DISLOCATION DENSITY BASED

An alternative choice on internal state variable could also be considered following the dislocation density based modelling approach of Estrin [2]. While the initial value of the true dislocation density values ($\rho_0 = \rho|_{\varepsilon_\text{p}=0}$) make the choice of dislocation density itself a difficult choice for an internal state variable, a stress like constant $\sigma_0 = \frac{1}{2}M\mu b\sqrt{\rho_0}$ is be introduced so that the threshold stress value is now determined from

$$\hat{\sigma}_\varepsilon = \sigma_0\sqrt{Y}. \tag{9}$$

This modification introduces the dislocation density ratio variable $Y = \frac{\rho}{\rho_0}$, a new internal state variable with typical initial value $Y|_{\varepsilon_\text{p}=0} = 1$. Equation (9) can be substituted into Equation (4) to formulate the MTS model in terms of the new internal state variable Y instead of the threshold stress value $\hat{\sigma}_\varepsilon$. Assuming no constant thermal stress component ($\hat{\sigma}_i = 0$MPa), the temperature and rate dependent flow stress in Equation (4) has the form

$$\sigma_\text{Y} = \hat{\sigma}_a + \sigma_0\sqrt{Y}\frac{\mu\,(T)}{\mu_r}S_\varepsilon(\dot{\varepsilon}_\text{p}, T). \tag{10}$$

The constitutive formulation may now be completed by using the theory on dislocation density based modelling to evolve the dislocation density ratio in the process of plastic deformation instead of the threshold stress directly. By introducing $C_1 = Mk_1/\sqrt{\rho_0}$ and $C_2\,(\dot{\varepsilon}_\text{p}, T) = Mk_2\,(\dot{\varepsilon}_\text{p}, T)$, evolution of the dislocation density ratio internal state variable following Equation (5b) is now determined from [2]

$$\frac{dY}{d\varepsilon_\text{p}} = C_1\sqrt{Y} - C_2(\dot{\varepsilon}_\text{p}, T)\,Y. \tag{11}$$

The evolution of the dislocation density ratio in Equation (11) is determined by different values of the constant C_1 and form of the the dynamic recovery annihilation function $C_2\,(\dot{\varepsilon}_\text{p}, T)$. We use a function

$$C_2(\dot{\varepsilon}_\text{p}, T) = C_{20}\exp\left[-\frac{T}{a_{02}\mu}\ln\left(\frac{\dot{\varepsilon}_\text{p}}{\dot{\varepsilon}_{02}}\right)\right], \tag{12}$$

that is equivalent to the saturation stress based formulation in Equation (8) used by Chen and Gray [12]. In this function C_{20}, $\dot{\varepsilon}_{02}$ and a_{02} are constants. a_{02} is a constant to represent the convenient grouping of parameters $a_{02} = g_{0s}b^3/k_{\mathrm{B}}$. Further inclusion of physical phenomena is possible by reformulating Equation (11).

Following the work done by Kok et al. [14] an evolving geometric substructure is included in the model by introducing the average slip plane lattice incompatibility $\bar{\lambda}$ as another internal state variable. Kok et al. [14] observed that the evolution of the average slip plane lattice incompatibility is inversely proportional to the grain size d_{x}. Using the proportionality constant C_λ, an evolution equation for this internal state variable is [14]

$$\frac{d\bar{\lambda}}{d\varepsilon_{\mathrm{p}}} = \frac{C_\lambda}{d_{\mathrm{x}}}. \tag{13}$$

Also using the formulation by Song and McDowell [15] as a further extension to the dislocation density ratio evolution equation, thermal recovery is added. The rate form of Equation (11) with large strain and thermal recovery effects is

$$\dot{Y} = \dot{\varepsilon}_{\mathrm{p}} \left(C_g \bar{\lambda}^{r_g} + C_1\sqrt{Y} - C_2(\dot{\varepsilon}_{\mathrm{p}}, T)\, Y \right) - C_3(T) Y^{r_3}. \tag{14}$$

where C_g, r_g and r_3 are constants while C_3 is a temperature dependent function. If the constant C_{30} is introduced while $a_{03} = Q_{\mathrm{self}}/R$ is associated with the scaled activation energy for self diffusion. The static or thermal recovery term is modelled using [15]

$$C_3(T) = C_{30} \exp\left(\frac{-a_{03}}{T} \right). \tag{15}$$

The dislocation density based model up to here is a physically extended form of the reformulated isotropic MTS model with large strain effects and static recovery using two evolving internal state variables (Y and $\bar{\lambda}$). Cyclic effects are now added to the model formulation. Some of the dislocations are recoverable in the event of load reversal, making it necessary to distinguish between truly immobilised and recoverable stored dislocation density. A non-dimensional form of the partially recoverable part of the dislocation density ratio is given by the internal state variable Z following the work done by Estrin [2]. This internal state variable evolves following

$$\dot{Z} = \dot{\varepsilon}_{\mathrm{p}} \left(C_4\sqrt{Y} - C_2(\dot{\varepsilon}_{\mathrm{p}}, T) Z \right) - C_5(T) Z. \tag{16}$$

Equation (16) contains a storage rate constant C_4 and dynamic recovery term $C_2(\dot{\varepsilon}_{\mathrm{p}}, T)Z$. $C_5(T)Z$ further represents the recoverable edge density loss rate due to thermally activated jog formation [2]. The last term is time rather than strain dependent and can take the form of the Arrhenius expression involving the activation energy for jog formation. Much like Equation (15), if $a_{05} = Q_{\mathrm{jog}}/R$ is used as a parameter representing the scaled activation energy associated with jog formation

$$C_5(T) = C_{50} \exp\left(\frac{-a_{05}}{T} \right). \tag{17}$$

The dislocation density variable Z is recovered upon each stress reversal. This corresponds to an internal state variable update

$$Y := Y - Z \qquad \text{and} \qquad Z := 0 \tag{18}$$

Estrin [2] further introduces a back stress σ_{B} into his chosen one dimensional kinetic equation. The evolution of the one dimensional back stress is considered to obey the equation

$$\frac{d\sigma_{\mathrm{B}}}{d\varepsilon_{\mathrm{p}}} = C_6\sqrt{Y} - C_7\sigma_{\mathrm{B}}, \tag{19}$$

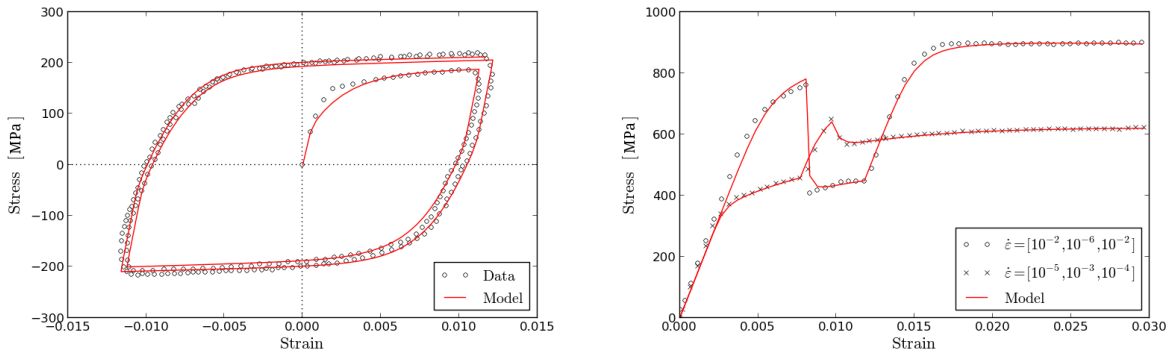

(a) (b)

Figure 2: (a) Cyclic data for Alloy 800H [2] versus the implemented model prediction. (b) Variable strain rate data for Inconel 738LC [2] versus model prediction.

where C_6 and C_7 are constants. The combined hardening model using Y, $\bar{\lambda}$, Z and back stress evolution equations is coded into a subroutine that works with the combined user material framework [8]. To illustrate the ability of the model, it is characterised to the deformation data for Alloy 800H and Inconel 738LC digitised from the work by Estrin [2].

Two cycles of the Alloy 800H material response is digitised and fit using the model. The deformation is modelled at 1123K and a strain rate of $2\times10^{-3}\text{s}^{-1}$. The model response fit to the digitised data is presented in Figure 2(a). The elastic parameter values of $\mu_r = 60$GPa, $\nu = 0.3$ and $D_r = 0$GPa so that $\mu = \mu_r$ are used. The athermal stress component is $\hat{\sigma}_a = 0$MPa while the reference stress parameter is $\sigma_0 = 734.41$MPa. Scaling factor parameter values are $a_{0\varepsilon} = g_{0\varepsilon}b^3/k_\text{B} = 0.7424$K/MPa, $p_\varepsilon = 0.5$, $q_\varepsilon = 1.5$ and $\dot{\varepsilon}_{0\varepsilon} = 10^7\text{s}^{-1}$. The other material parameter values are $C_g = 0$, $C_{30} = 0\text{s}^{-1}$, $C_1 = 43.302$, $C_{20} = 32.469$, $a_{02} = 4.497$K/MPa, $\dot{\varepsilon}_{02} = 10^7\text{s}^{-1}$, $C_4 = 10.589$, $C_{50} = 0.7253\text{s}^{-1}$ and $a_{05} = 20000$K with the parameters associated with the back stress evolution $C_6 = 64897.42$MPa and $C_7 = 628.34$.

In Figure 2(b), the model prediction is presented along with the variable strain rate data for Inconel 738LC. In this case, the elastic parameter values of $\mu_r = 50$GPa, $\nu = 0.3$ and $D_r = 0$GPa are used. The athermal stress component is $\hat{\sigma}_a = 277.184$MPa with $\sigma_0 = 4410.47$MPa. Scaling factor parameter values are $a_{0\varepsilon} = 0.9392$K/MPa, $p_\varepsilon = 0.2551$, $q_\varepsilon = 0.755$ and $\dot{\varepsilon}_{0\varepsilon} = 10^7\text{s}^{-1}$. Furthermore $C_g = 0$, $C_{30} = 0\text{s}^{-1}$, $C_1 = 22.23$, $C_{20} = 75.67$, $a_{02} = 0.478$K/MPa, $\dot{\varepsilon}_{02} = 10^7\text{s}^{-1}$, $C_4 = 0.0039$, $C_{50} = 11.924\text{s}^{-1}$ and $a_{05} = 20000$K. The back stress is evolved using $C_6 = 30329.65$MPa and $C_7 = 180.11$.

There is a good fit despite setting $C_g = 0$ and therefore ignoring the effect of $\bar{\lambda}$ on the dislocation density accumulation. This indicates that the carbide particles present in the alloy does not affect the cyclic behaviour of the material according to the data used. If more data is available at different rates and temperatures during the model characterisation, the parameter values should have other values since the Alloy 800H cyclic data is at isothermal conditions for a single rate for example.

RECRYSTALLISATION

A recrystallisation model similar to the one validated by Brown and Bammann [3] is implemented. Multiple waves of recrystallisation can be simulated with various recrystallised and unrecrystallised volume fractions existing simultaneously. The recrystallisation is based on the mobility of grain and subgrain boundaries. From the work by Cahn and Hagel [16], the recrystallised volume fraction growth rate is

$$\dot{f}_\text{x} = A_\text{x} v_\text{x}. \tag{20}$$

Here, A_{x} is the interfacial area between recrystallised and unrecrystallised regions and v_{x} is the average velocity of the interface. Average grain boundary velocity is calculated using [17]

$$v_{\mathrm{x}} = MP, \tag{21}$$

where M is the grain boundary mobility and P the driving pressure. As the material deforms, the average misorientation across the geometrically necessary subgrain boundaries increase, which in turn increases the mobility of the boundaries. In the dislocation density ratio based model implementation, the average slip plane lattice misorientation $\bar{\lambda}$ internal state variable is assumed proportional to the average misorientation angle $\bar{\theta}$ [8]. The misorientation angle ratio used by Chen et al. [18] is therefore replaced and a reformulated equation using the average lattice slip plane incompatibility is introduced. The average subgrain boundary mobility is approximated as [8]

$$\bar{M} = M_0 \exp\left(-\frac{Q_M}{RT}\right)\left[1 - \exp\left(-C_{M\theta}\bar{\lambda}^{r_{M\theta}}\right)\right] \tag{22}$$

where Q_M is the activation energy for grain boundary mobility while M_0, $C_{M\theta}$ and $r_{M\theta}$ are constants. The pressure driving the subgrain boundary growth can in it's simplest form be expressed as $P = \frac{1}{2}\mu b^2 \rho$ [19]. Considering the dislocation density ratio used as evolving internal state variable, $Y = \rho/\rho_0$, the driving pressure is calculated by

$$P = \frac{1}{2}\mu b^2 \rho_0 Y. \tag{23}$$

Equations(22) and (23) means recrystallisation is modelled in terms of the internal state variables Y and $\bar{\lambda}$. An isotropic implementation using these two state variables is therefore considered.

The original unrecrystallised material has a volume fraction $f_{\mathrm{x}_0} = 1$. f_{x_1} represents the material volume fraction that has undergone one recrystallisation cycle while the remaining unrecrystallised volume fraction is $1 - f_{\mathrm{x}_1}$. Given multiple cycles of recrystallisation, $f_{\mathrm{x}_i} - f_{\mathrm{x}_{i+1}}$ represents the total volume fraction of material that has been recrystallised i times as in the model by Brown and Bammann [3]. Each volume fraction has it's own set of internal state variables. The variables Y_{x_i} and $\bar{\lambda}_{\mathrm{x}_i}$ represent the internal state variables associated with the material volume fraction $f_{\mathrm{x}_i} - f_{\mathrm{x}_{i+1}}$. The interfacial boundary area A_{x} in Equation (20) is approximated between the f_{x_i} and $f_{\mathrm{x}_{i+1}}$ volume fractions using the equation formulated by Brown and Bammann [3]

$$A(f_{\mathrm{x}_i}, f_{\mathrm{x}_{i+1}}) = f_{\mathrm{x}_i}\left(\frac{f_{\mathrm{x}_{i+1}}}{f_{\mathrm{x}_i}}\right)^{r_{\mathrm{Rx}a}}\left(1 - \frac{f_{\mathrm{x}_{i+1}}}{f_{\mathrm{x}_i}}\right)^{r_{\mathrm{Rx}b}}\left(1 + C_{\mathrm{Rx}c}\left(1 - f_{\mathrm{x}_i}\right)\right), \tag{24}$$

where $r_{\mathrm{Rx}a}$, $r_{\mathrm{Rx}b}$ and $C_{\mathrm{Rx}c}$ are constants. Using Equations (22), (23) and (24) a generalised recrystallised volume fraction growth rate for $f_{\mathrm{x}_{i+1}}$ is formulated using the state variables for the volume fraction $f_{\mathrm{x}_i} - f_{\mathrm{x}_{i+1}}$. Equation (20) is formulated for each $f_{\mathrm{x}_{i+1}}$ as

$$\dot{f}_{\mathrm{x}_{i+1}} = Y_{\mathrm{x}_i} C_{\mathrm{Rx}0} C_{\mathrm{Rx}T}(T) C_{\mathrm{Rx}\lambda}\left(\bar{\lambda}_{\mathrm{x}_i}\right) A(f_{\mathrm{x}_i}, f_{\mathrm{x}_{i+1}}). \tag{25}$$

The function is written so that $C_{\mathrm{Rx}0}$ effectively contains all the pre-exponential constants. Similarly, $C_{\mathrm{Rx}T}(T)$ contains the temperature dependence in a single function

$$C_{\mathrm{Rx}T}(T) = \mu\left(T\right)\exp\left(-\frac{a_{0\mathrm{Rx}}}{T}\right). \tag{26}$$

Here, $a_{0\mathrm{Rx}}$ is again the convenient grouping of the activation energy and universal gas constant as done in Equation (15). The function $C_{\mathrm{Rx}\lambda}\left(\bar{\lambda}\right)$ contains the geometric effects in the rewritten function

$$C_{\mathrm{Rx}\lambda}\left(\bar{\lambda}_{\mathrm{x}_i}\right) = 1 - \exp\left(-C_{\mathrm{Rx}\lambda 0}\bar{\lambda}_{\mathrm{x}_i}^{r_{\mathrm{Rx}\lambda}}\right), \tag{27}$$

where $C_{\mathrm{Rx}\lambda 0}$ and $r_{\mathrm{Rx}\lambda}$ replaces the constant $C_{M\theta}$ and exponent $r_{M\theta}$ in Equation (22) for subscript consistency.

Given a time increment δt, the first (f_{x_1}) and second (f_{x_2}) volume fractions can both progress, meaning region $f_{\mathrm{x}_1} - f_{\mathrm{x}_2}$ will increase by δf_{x_1} and decrease by δf_{x_2}. Assuming recrystallisation removes the dislocation structure, the dislocation density ratio within a newly recrystallised portion δf_{x_1} should be reset. This is taken into account by Brown and Bammann [3] using the rule of mixtures. Doing the same for the model in Jansen van Rensburg [8], the dislocation density ratio evolution in Equation (14) is replaced by

$$\dot{Y}_{\mathrm{x}_i} = \dot{\varepsilon}_{\mathrm{p}} \left(C_g \bar{\lambda}_{\mathrm{x}_i}^{r_g} + C_1 \sqrt{Y_{\mathrm{x}_i}} - C_2(\dot{\varepsilon}_{\mathrm{p}}, T)\, Y_{\mathrm{x}_i} \right) - C_3(T) Y_{\mathrm{x}_i}^{r_3} - \frac{\dot{f}_{\mathrm{x}_i}}{f_{\mathrm{x}_i} - f_{\mathrm{x}_{i+1}}} Y_{\mathrm{x}_i} \tag{28}$$

for the dislocation density ratio associated with volume fraction $f_{\mathrm{x}_i} - f_{\mathrm{x}_{i+1}}$. The average slip plane lattice incompatibility in Equation (13) is also replaced in the presence of recrystallisation by

$$\dot{\bar{\lambda}}_{\mathrm{x}_i} = \dot{\varepsilon}_{\mathrm{p}} C_{\lambda \mathrm{x}} - \frac{\dot{f}_{\mathrm{x}_i}}{f_{\mathrm{x}_i} - f_{\mathrm{x}_{i+1}}} \bar{\lambda}_{\mathrm{x}_i} \tag{29}$$

for the $f_{\mathrm{x}_i} - f_{\mathrm{x}_{i+1}}$ material volume fraction. $C_{\lambda \mathrm{x}}$ here is a constant related to $C_\lambda / d_{\mathrm{x}}$ in Equation (13) if the grain size itself is not specifically known. In the presence of recrystallisation, the equivalent threshold stress of Equation (9) is calculated using the average dislocation density ratio

$$\bar{Y} = \sum_{i=0}^{n_{\mathrm{x}}-1} Y_{\mathrm{x}_i} \left(f_{\mathrm{x}_i} - f_{\mathrm{x}_{i+1}} \right), \tag{30}$$

where n_{x} is the total number of recrystallisation cycles. The dislocation density based user material with recrystallisation is implemented into a subroutine called by the isotropic user material framework [8]. The model is illustrated here on a larger set of the Copper data digitised from the experimental work done by Tanner and McDowell [13]. The material parameters resulting in the fit to the Copper data in Figure 3 are:

- μ_r = 43.8GPa, D_r = 4.7GPa, T_r = 252K and ν = 1/3 for the elastic properties using the shear model relationship in Equation (2).
- $a_{0\varepsilon} = g_{0\varepsilon} b^3 / k_{\mathrm{B}}$ =2.1037K/MPa, $p_\varepsilon = 1$, $q_\varepsilon = 2$, and $\dot{\varepsilon}_{0\varepsilon}$ =$10^6 \mathrm{s}^{-1}$ for the temperature and rate dependent scaling function in (3).
- The athermal yield stress component is $\hat{\sigma}_a$ =12.519MPa and reference stress is σ_0 = 17.295MPa using Equation (10).
- $C_{\lambda \mathrm{x}} = 1$ is used for the evolution of $\bar{\lambda}$ according to Equation (29).
- C_g = 6378.74, r_g = 0.769, C_1 = 278.87, C_{20} = 11.773, a_{02} = 0.904K/MPa, $\dot{\varepsilon}_{02}$ = 4.0112×10^{12}, C_{30} = 83.07s^{-1}, a_{03} = 6370.675K and r_3 =0.8079 for the dislocation density ratio evolution in Equation (28).
- $C_{\mathrm{Rx}0}$ = 9346.62s^{-1} in Equation (25), $a_{0\mathrm{Rx}}$ =17633.796K in Equation (26) while $C_{\mathrm{Rx}\lambda 0}$ = 47.247 and $r_{\mathrm{Rx}\lambda}$ = 3.87 in Equation (27). $r_{\mathrm{Rx}a}$ = 0.1424, $r_{\mathrm{Rx}b}$ = 1.7677 and $C_{\mathrm{Rx}c}$ = 393.44 in Equation (24).

The model gives valid responses in a large range of rates and temperatures as visible in Figure 3 with temperatures ranging from 25°C to 541°C and rates between 0.0004s^{-1} and 6000s^{-1}. Thanks to the user material framework [8] it is also possible to use the recrystallisation model in a finite element simulation. In Figure 4, different internal state variables are displayed as a result of a simulation using the material parameters identified for Copper.

Compression of a Copper billet is modelled using an axi-symmetric simulation. A billet with diameter 5mm and height 7.5mm is compressed to 50% its original height in 2000 seconds. The compression is modelled at a constant temperature of 541°C. In Figure 4(a) the equivalent dislocation density using Equation (30) is illustrated with the volume fraction averaged slip plane lattice misorientation (b). Figure 4(c) shows the volume fraction recrystallised at least once while Figure 4(d) shows the material volume fraction that has undergone at least two recrystallisation cycles.

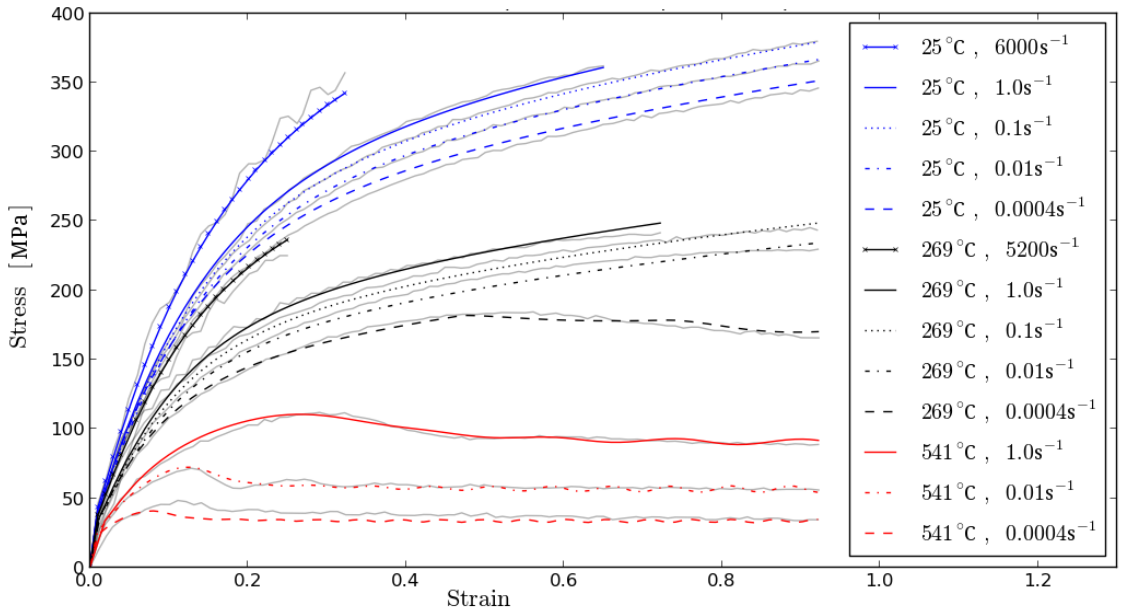

Figure 3: Numerical model (colored lines) calibrated to Tanner and McDowell's OFHC copper data [13] for different strain rates at 25°C, 269°C and 541°C.

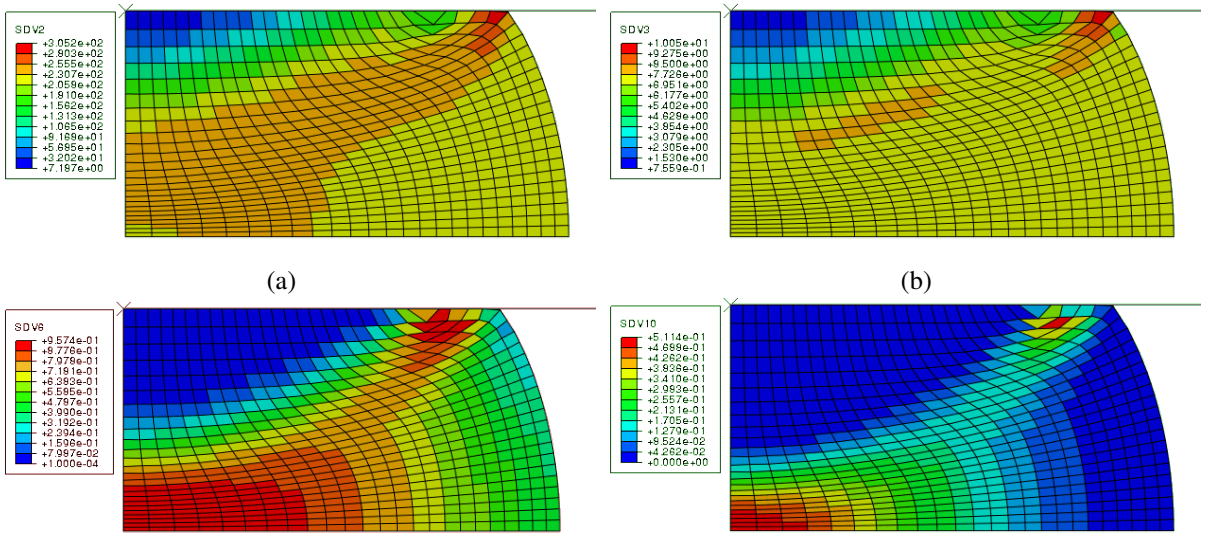

Figure 4: Internal state variables of a billet with recrystallisation compressed 50% in 2000 seconds at 541°C. (a) Equivalent dislocation density ratio and (b) Misorientation. Volume fractions associated with (c) the first and (d) second wave of recrystallisation.

CONCLUSIONS

Thanks to the incrementally objective user material frameworks [8], sophisticated state dependent material models can be implemented into a finite element environment. Different model formulations are possible by altering the Fortran code called to represent the relevant one dimensional model formulation. This was illustrated using the MTS model as well as models for dislocation density based combined hardening and isotropic hardening with recrystallisation as an example [8].

REFERENCES

1 Follansbee, P. S. and Kocks, U. F., "A constitutive description of copper based on the use of the mechanical threshold stress as an internal state variable", Vol. 36, No. 1, pp. 81 – 93, Acta Materialia, 1998.

2 Estrin, Y., "Dislocation-density-related constitutive modeling", In: Krausz, A. and Krausz, K. (Eds.), Unified constitutive laws of plastic deformation, Ch. 2, pp. 69 – 106, Academic Press, San Diego, 1996.

3 Brown, A. A. and Bammann, D. J., "Validation of a model for static and dynamic recrystallization in metals", Vol. 32-33, pp. 17 – 35, International Journal of Plasticity, 2012.

4 Kocks, U. F., Argon, A. S., and Ashby, M. F., "Thermodynamics and Kinetics of Slip", In: Progress in Materials Science, Vol. 19, Pergamon, Oxford, 1975.

5 Kocks, U. F., "Laws for work-hardening and low temperature creep", Vol. 98, pp. 76 – 85, Journal of Engineering Materials and Technology, 1976.

6 Kocks, U. F. and Mecking, H., "A mechanism for static and dynamic recovery", In: Haasen, P., Gerold, V., and Korstorz, G. (Eds.), Strength of Metals and Alloys, pp. 345 – 350, Pergamon, Oxford, 1979.

7 Mecking, H. and Kocks, U. F., Vol. 29, pp. 1865 – 1877, Acta Materialia, 1981.

8 Jansen van Rensburg, G. J., "Development and Implementation of State Variable Based User Materials in Computational Plasticity", Unpublished Thesis, University of Pretoria, 2016.

9 Nabarro, F. R. N., Basinski, Z. S., and Holt, D. B., "The plasticity of pure single crystals", Vol. 13, No. 50, pp. 193 – 323, Advances in Physics, 1964.

10 Varshni, Y. P., "Temperature dependence of the elastic constants", Vol. 2, No. 10, pp. 3952 – 3958, Physical Review B, 1970.

11 Kocks, U. F., Tomé, C., and Wenk, H., Texture and Anisotropy, Cambridge University Press, 1998.

12 Chen, S. R. and Gray, G. T., "Constitutive behavior of tantalum and tantalum-tungsten alloys", Vol. 27A, pp. 2994 – 3006, Metallurgical and Materials Transactions A, 1996.

13 Tanner, A. B. and McDowell, D. L., "Deformation, temperature and strain rate sequence experiments on OFHC Cu", Vol. 15, No. 4, pp. 375 – 399, International Journal of Plasticity, 1999.

14 Kok, S., Beaudoin, A. J., and Tortorelli, D. A., "On the development of stage IV hardening using a model based on the mechanical threshold", Vol. 50, No. 7, pp. 1653 – 1667, Acta Materialia, 2002.

15 Song, J. E. and McDowell, D. L., Grain Scale Crystal Plasticity Model with Slip and Microtwinning for a Third Generation Ni-Base Disk Alloy, pp. 159 – 166, John Wiley & Sons, Hoboken, 2012.

16 Cahn, J. W. and Hagel, W. C., "Theory of the pearlite reaction", pp. 131 – 196, Decomposition of Austenite by Diffusional Processes, 1962.

17 Doherty, R. D., Hughes, D. A., Humphreys, F. J., Jonas, J. J., Juul Jensen, D., Kassner, M. E., King, W. E., McNelley, T. R., McQueen, H. J., and Rollett, A. D., "Current issues in recrystallization: A review", Vol. 238, No. 2, pp. 219 – 274, Materials Science and Engineering A, 1997.

18 Chen, S. P., Zwaag, S., and Todd, I., "Modeling the kinetics of grain-boundary-nucleated recrystallization processes after cold deformation", Vol. 33, No. 3, pp. 529 – 537, Metallurgical and Materials Transactions A, 2002.

19 Humphreys, F. J. and Hatherly, M., Recrystallization and Related Annealing Phenomena, Elsevier, 2nd Edition, 1995.